iScience

CellPress

Article

Ezh1 Targets Bivalent Genes to Maintain Self-Renewing Stem Cells in *Ezh2*-Insufficient Myelodysplastic Syndrome

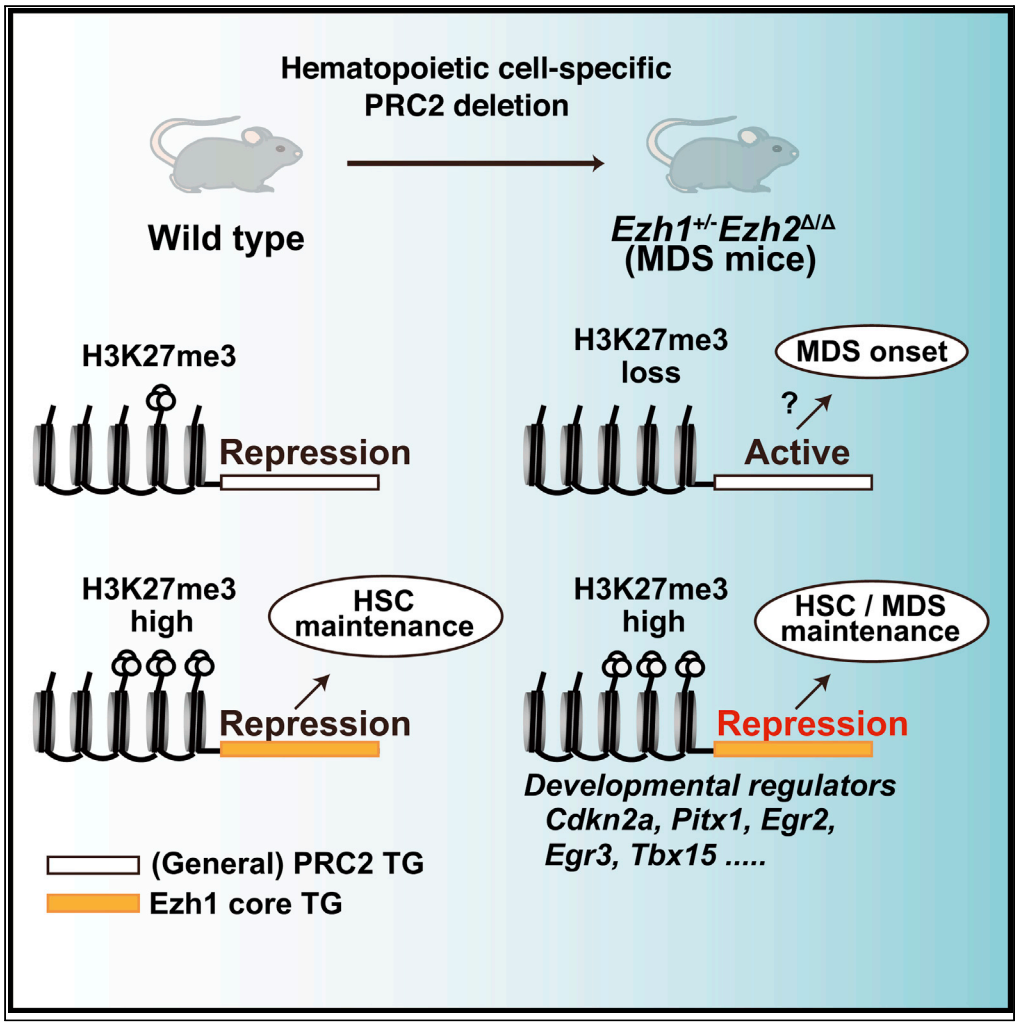

Kazumasa Aoyama, Motohiko Oshima, Shuhei Koide, ..., Yaeko Nakajima-Takagi, Goro Sashida, Atsushi Iwama

aoyamakazumasa@chiba-u.jp (K.A.)
03aiwama@ims.u-tokyo.ac.jp (A.I.)

HIGHLIGHTS

One allele of *Ezh1* is enough to maintain self-renewing HSCs and MDS stem cells

Ezh1 core targets are marked with high levels of H3K27me3 and H2AK119ub1 in HSPCs

Ezh1 core targets are mostly bivalent developmental regulators and critical for HSCs

Aoyama et al., iScience 9, 161–174
November 30, 2018 © 2018 The Author(s).
https://doi.org/10.1016/j.isci.2018.10.008

iScience

CellPress

Article

Ezh1 Targets Bivalent Genes to Maintain Self-Renewing Stem Cells in *Ezh2*-Insufficient Myelodysplastic Syndrome

Kazumasa Aoyama,[1,*] Motohiko Oshima,[1] Shuhei Koide,[1] Emi Suzuki,[1] Makiko Mochizuki-Kashio,[1] Yuko Kato,[1] Shiro Tara,[1] Daisuke Shinoda,[1] Nobuhiro Hiura,[1] Yaeko Nakajima-Takagi,[1] Goro Sashida,[1,2] and Atsushi Iwama[1,3,4,*]

SUMMARY

Polycomb repressive complex (PRC) 2 represses transcription through histone H3K27 trimethylation (H3K27me3). We previously reported that the hematopoietic-cell-specific deletion of *Ezh2*, encoding a PRC2 enzyme, induced myelodysplastic syndrome (MDS) in mice, whereas the concurrent *Ezh1* deletion depleted hematopoietic stem and progenitor cells (HSPCs). We herein demonstrated that mice with only one *Ezh1* allele (*Ezh1*$^{+/-}$*Ezh2*$^{\Delta/\Delta}$) maintained HSPCs. A chromatin immunopreciptation sequence analysis revealed that residual PRC2 preferentially targeted genes with high levels of H3K27me3 and H2AK119 monoubiquitination (H2AK119ub1) in HSPCs (designated as Ezh1 core target genes), which were mostly developmental regulators, and maintained H3K27me3 levels in *Ezh1*$^{+/-}$*Ezh2*$^{\Delta/\Delta}$ HSPCs. Even upon the complete depletion of *Ezh1* and *Ezh2*, H2AK119ub1 levels were largely retained, and only a minimal number of Ezh1 core targets were de-repressed. These results indicate that genes marked with high levels of H3K27me3 and H2AK119ub1 are the core targets of polycomb complexes in HSPCs as well as MDS stem cells.

INTRODUCTION

Polycomb-group proteins are responsible for the regulation of gene expression by catalyzing repressive histone modifications. They form several types of complexes, including Polycomb repressive complex 2 (PRC2) and PRC1, which are responsible for histone H3 lysine 27 mono-, di-, and tri-methylation (H3K27me1/2/3) and H2AK119 mono-ubiquitination (H2AK119ub1), respectively. PRC2 consists of EED, SUZ12, and the PRC2 enzymatic component, enhancer of zeste homolog 2 (EZH2). PRC2-mediated H3K27me3 plays critical roles in the stage-specific repression of developmental regulator genes, which frequently exhibits bivalency with an active histone modification, H3K4me3, during cellular differentiation. The deregulation of this system has been observed in various types of cancers (Conway et al., 2015; Margueron and Reinberg, 2011).

EZH1 is another enzymatic component of PRC2 and has a catalytic SET domain showing high homology to that of *EZH2*. The H3K27me2/3 activity of EZH1 is markedly weaker than that of EZH2 *in vivo* (Margueron et al., 2008), and, consistent with this finding, no mutation in *EZH1* has been identified, at least in hematological malignancies. The biological importance of EZH1 is considered to be as a backup enzyme for EZH2, which compensates for EZH2 deficiencies in transcriptional repression in embryonic stem (ES) cells, skin stem cells, and hematopoietic cells (Ezhkova et al., 2011; Margueron et al., 2008; Mochizuki-Kashio et al., 2015; Shen et al., 2008). In addition, several groups have revealed that EZH1 forms a non-canonical PRC2 complex that is associated with active transcription (Henriquez et al., 2013; Mousavi et al., 2012; Stojic et al., 2011; Xu et al., 2015). Another intriguing but controversial issue would be the tissue-specific compensation between EZH1 and EZH2.

PRC2-mediated H3K27me3 cooperates with H2AK119ub1 to repress gene expression. H2AK119ub1 is the epigenetic modification catalyzed by canonical and variant (non-canonical) PRC1s, which contain a RING finger E3 ligase, Ring1B or Ring1A, as the enzymatic component. H2AK119ub1 functions down- and upstream of H3K27me3. In the well-established model, PRC2-induced H3K27me3 recruits canonical PRC1, containing CBX as the H3K27me3-binding module. On the other hand, recent studies have reported the existence of variant PRC1s, which lack CBX proteins but bind to a stretch of unmethylated CpG sites

[1]Department of Cellular and Molecular Medicine, Graduate School of Medicine, Chiba University, 1-8-1 Inohana, Chuo-ku, Chiba 260-8670 Japan

[2]International Research Center for Medical Sciences, Kumamoto University, Kumamoto 860-0811, Japan

[3]Division of Stem Cell and Molecular Medicine, Center for Stem Cell Biology and Regenerative Medicine, Institute of Medical Science, University of Tokyo, 4-6-1 Shirokanedai, Minato-ku, Tokyo 108-8639, Japan

[4]Lead Contact

*Correspondence: aoyamakazumasa@chiba-u.jp (K.A.), 03aiwama@ims.u-tokyo.ac.jp (A.I.)

https://doi.org/10.1016/j.isci.2018.10.008

This is an open access article under the CC BY-NC-ND license (http://creativecommons.org/licenses/by-nc-nd/4.0/).

and induce H2AK119ub1, independently of PRC2 (Blackledge et al., 2015; Holoch and Margueron, 2017; Kondo et al., 2016).

Comprehensive genome sequencing studies identified change-of-function mutations in *EZH2*, which increase H3K27me3 levels and reduce H3K27me2 levels, in patients with follicular and diffuse large B-cell lymphomas (Morin et al., 2010). Loss-of-function mutations in *EZH2* have also been identified in patients with myelodysplastic syndrome (MDS) (3%–13%), myeloproliferative neoplasms (MPN) (3%–13%), and MDS/MPN overlap disorders (8%–15.6%), which are all clonal myeloid disorders originating from HSCs (Iwama, 2017; Sashida and Iwama, 2017). Since *EZH2* is located at chromosome 7q36.1, chromosomal abnormalities, such as −7 and 7q-, result in deletions of *EZH2* in hematological malignancies (Honda et al., 2015). We demonstrated using mice models that the hematopoietic-cell-specific deletion of *Ezh2* caused a number of hematological malignancies, such as MDS, MDS/MPN, and MPN (Mochizuki-Kashio et al., 2015; Muto et al., 2013; Sashida et al., 2014, 2016). Collectively, these findings suggest a tumor suppressor role for *EZH2* in hematological malignancies. Furthermore, we found that in the absence of *Ezh1*, the loss of *Ezh2* did not induce any hematological malignancies due to the exhaustion of hematopoietic stem cells (HSCs). These findings showed that *Ezh1* plays an essential role in *Ezh2*-insufficient MDS and that at least either Ezh1 or Ezh2 is required for normal HSC maintenance (Mochizuki-Kashio et al., 2015). The requirement of PRC2 for HSC maintenance has been reported in another mouse model in which *Eed* was deleted in a hematopoietic-cell-specific manner (Xie et al., 2014). *Cdkn2a* was identified as one of the critical target genes (TG) of PRC2 for HSC function because its deletion partially rescued the exhaustion of *Eed*-deleted HSCs, implying the existence of other PRC2 targets involved in HSC maintenance. However, the molecular mechanism underlying *Ezh1*-mediated maintenance of HSCs and MDS stem cells in an *Ezh2*-insufficient setting has not been addressed.

In the present study, we deleted all genes encoding PRC2 enzymatic components, except for a single allele of *Ezh1*, in hematopoietic cells in mice ($Ezh1^{+/-}Ezh2^{\Delta/\Delta}$). Using these mice, we revealed that a single allele of *Ezh1* is enough for *Ezh2*-insufficient MDS development. We profiled Ezh1 core TG, which are critical for the maintenance of HSCs as well as MDS stem cells. Furthermore, H2AK119ub1 mediated by PRC1 has been suggested to contribute to the transcriptional repression of Ezh1 core TG in the setting of a PRC2 insufficiency.

RESULTS

$Ezh1^{+/-}Ezh2^{\Delta/\Delta}$ Mice Maintain HSC Functions

We previously reported that $Ezh2^{\Delta/\Delta}$ mice developed heterogeneous hematological malignancies, mostly MDS and MDS/MPN, whereas $Ezh1^{-/-}Ezh2^{\Delta/\Delta}$ (DKO) mice did not develop any disease due to the exhaustion of HSCs (Mochizuki-Kashio et al., 2015). These findings clearly indicated an important role for *Ezh1* in the maintenance of HSCs and tumor-initiating cells in the setting of an *Ezh2* insufficiency. To clarify the function of *Ezh1* in hematopoiesis and MDS, we generated $Ezh1^{+/-}Ezh2^{fl/fl}$ mice to analyze the impact of a one-allele loss of *Ezh1* in $Ezh2^{\Delta/\Delta}$ mice. Bone marrow (BM) cells from *Cre-ERT* control, *Cre-ERT*; $Ezh1^{-/-}$, *Cre-ERT*; $Ezh2^{fl/fl}$, and *Cre-ERT*; $Ezh1^{+/-}Ezh2^{fl/fl}$ mice (CD45.2) were transplanted into lethally irradiated CD45.1 recipient mice. *Ezh2* was deleted by intraperitoneal injections of tamoxifen 1 month post-transplantation (Figure 1A). We hereafter refer to recipient mice reconstituted with *Cre-ERT* control, *Cre-ERT*; $Ezh1^{-/-}$, *Cre-ERT*; $Ezh2^{fl/fl}$, and *Cre-ERT*; $Ezh1^{+/-}Ezh2^{fl/fl}$ cells as wild-type (WT), $Ezh1^{-/-}$, $Ezh2^{\Delta/\Delta}$, and $Ezh1^{+/-}Ezh2^{\Delta/\Delta}$ mice, respectively. Genomic PCR and RNA sequencing (RNA-seq) analyses confirmed the efficient deletion of *Ezh2* in $Ezh2^{\Delta/\Delta}$ and $Ezh1^{+/-}Ezh2^{\Delta/\Delta}$ mice (Figures 1B and 1C). RNA-seq revealed that *Ezh1* mRNA levels were reduced by approximately 50% in $Ezh1^{+/-}Ezh2^{\Delta/\Delta}$ cells (Figure 1B). A western blot analysis confirmed reductions in the global levels of tri- and di-methylation at histone H3 lysine 27 (H3K27me3 and me2) and the methylation to acetylation switch at H3K27 (Pasini et al., 2010) in $Ezh2^{\Delta/\Delta}$ and $Ezh1^{+/-}Ezh2^{\Delta/\Delta}$ cells. The loss of one *Ezh1* allele had a minimal impact on the global levels of histone modifications at H3K27 (Figure 1D). Intriguingly, the chimerism of $Ezh1^{+/-}Ezh2^{\Delta/\Delta}$ donor cells, like that of WT, $Ezh1^{-/-}$, and $Ezh2^{\Delta/\Delta}$ mice, was almost 100% in peripheral blood (PB) at least for 6 months after *Ezh2* deletion (Figure 1E). $Ezh1^{+/-}Ezh2^{\Delta/\Delta}$ mice showed morphological dysplasia in PB cells (Figure 1F) as $Ezh2^{\Delta/\Delta}$ mice did (Mochizuki-Kashio et al., 2015), and also showed macrocytic anemia, leukopenia, and increased apoptosis of BM erythroblasts (data not shown). These results indicate that $Ezh1^{+/-}Ezh2^{\Delta/\Delta}$ mice developed MDS and maintained MDS stem cells as well as HSCs for a long term.

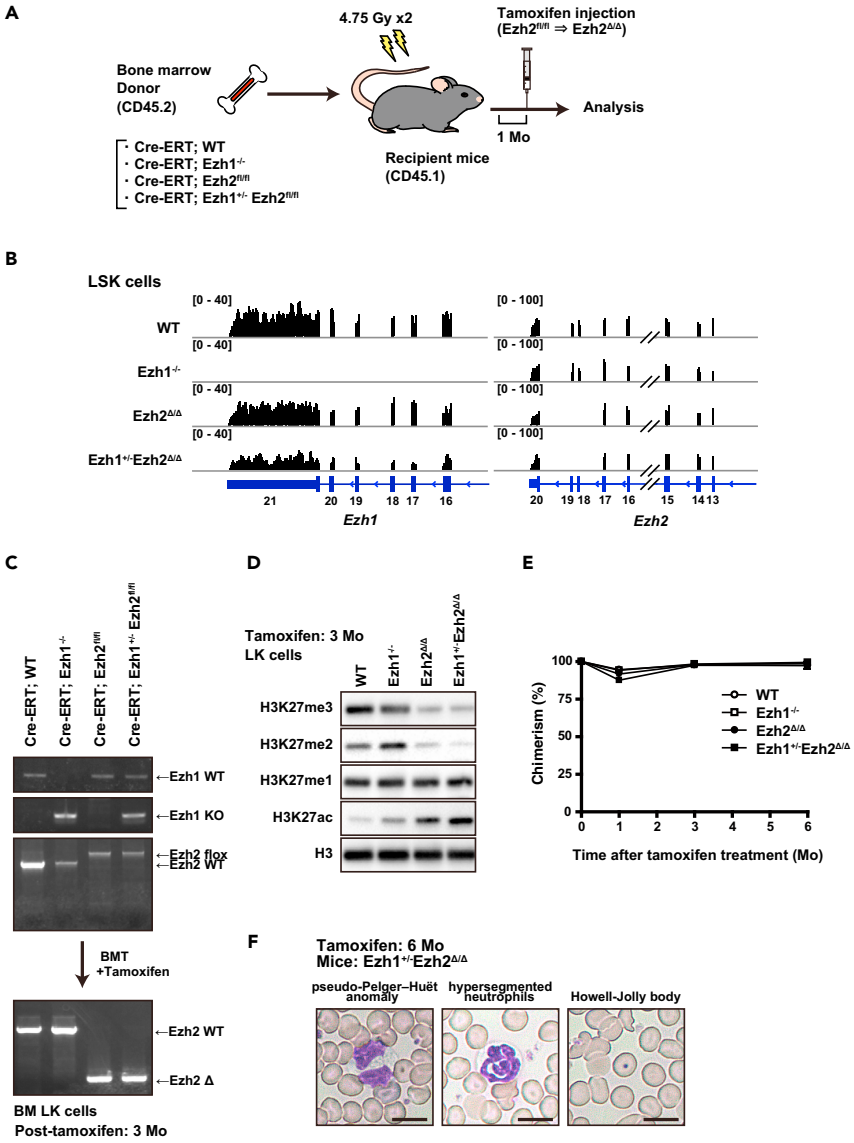

Figure 1. Efficient Deletion of *Ezh1* and *Ezh2* in Hematopoietic Cells

(A) The experimental scheme of BM transplantation (BMT) and hematopoietic-cell-specific deletion of *Ezh1* and *Ezh2*.

(B) Snapshots of RNA-seq signals at *Ezh1* and *Ezh2* gene loci in $Lin^{-}Sca\text{-}I^{+}c\text{-}Kit^{+}$ cells (LSK cells) obtained from WT, $Ezh1^{-/-}$, $Ezh2^{\Delta/\Delta}$, and $Ezh1^{+/-}Ezh2^{\Delta/\Delta}$ recipient mice 3 months (Mo) after the tamoxifen treatment.

(C) Genomic PCR on $Lin^{-}c\text{-}Kit^{+}$ cells (LK cells) isolated as described in (B), using the tail genomic DNA of donor mice as control.

(D) Western blot analysis of global histone modification levels in hematopoietic progenitor cells (HPCs). LK cells isolated as described in (B) were subjected to a western blot analysis using anti-H3K27me3, H3K27me2, H3K27me1, H3K27ac, and histone H3 antibodies.

(E) The chimerism of donor-derived $CD45.2^{+}$ cells in the PB of recipient mice.

(F) Smear preparation of PB from WT and $Ezh1^{+/-}Ezh2^{\Delta/\Delta}$ mice 6 months after the deletion of *Ezh2* observed after May-Giemsa staining. Scale bar, 10 μm.

To further assess the HSC function of $Ezh1^{+/-}Ezh2^{\Delta/\Delta}$ HSCs, we first performed competitive repopulating assays (Figure 2A). BM cells from each genotype were transplanted with a half number of $CD45.1^{+}$ competitor cells. Although the chimerism of $Ezh1^{+/-}Ezh2^{\Delta/\Delta}$ donor cells was slightly lower than that of $Ezh2^{\Delta/\Delta}$ donor cells in PB, $Ezh1^{+/-}Ezh2^{\Delta/\Delta}$ donor cells maintained hematopoiesis for a long term (Figure 2B). In contrast, DKO donor cells were totally outcompeted by competitor cells. We then performed serial

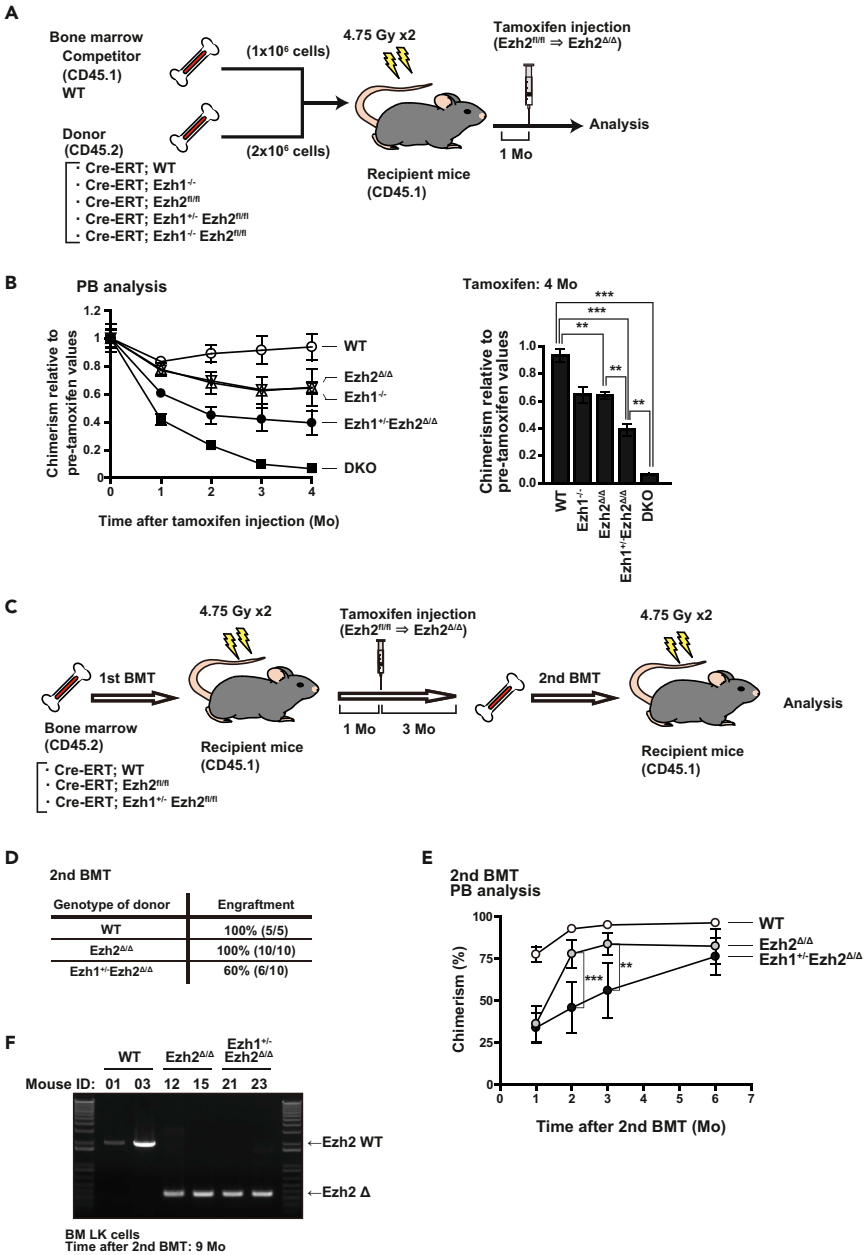

Figure 2. *Ezh1*$^{+/-}$*Ezh2*$^{\Delta/\Delta}$ Mice Maintain HSC Functions

(A) The experimental scheme of competitive repopulating assays. Two million BM cells (CD45.2) from *Cre-ERT*, *Cre-ERT;Ezh1*$^{-/-}$, *Cre-ERT;Ezh2*$^{fl/fl}$, and *Cre-ERT;Ezh1*$^{+/-}$*Ezh2*$^{fl/fl}$ were transplanted into lethally irradiated recipient mice (CD45.1) with 1 × 10^6 competitor BM cells (CD45.1), and *Ezh2* was then deleted by injecting tamoxifen 1 month (Mo) post-transplantation.

(B) The chimerism of donor-derived CD45.2$^+$ cells in the PB of recipient mice is shown as the ratio of chimerism values before treatment with tamoxifen (left panel). The chimerism 4 months after the tamoxifen treatment is summarized in a bar graph (right panel). Data are shown as the mean ± SD (WT, n = 4; *Ezh1*$^{-/-}$, n = 5; *Ezh2*$^{\Delta/\Delta}$, n = 3; *Ezh1*$^{+/-}$*Ezh2*$^{\Delta/\Delta}$, n = 4; *Ezh1*$^{-/-}$*Ezh2*$^{\Delta/\Delta}$, n = 4).

(C) The experimental scheme of serial BM transplantation (BMT). For secondary transplantation, 5 × 10^6 BM cells from primary recipient mice 3 months after tamoxifen treatment were transplanted into lethally irradiated secondary recipient mice.

(D) A summary of the engraftment rates of donor cells in secondary transplantation.

(E) The chimerism of donor-derived CD45.2$^+$ cells in PB in secondary recipients. Data are shown as the mean ± SD (WT, n = 5; *Ezh2*$^{\Delta/\Delta}$, n = 9; *Ezh1*$^{+/-}$*Ezh2*$^{\Delta/\Delta}$, n = 5).

(F) Genomic PCR of LK cells obtained from WT, *Ezh2*$^{\Delta/\Delta}$, and *Ezh1*$^{+/-}$*Ezh2*$^{\Delta/\Delta}$ recipient mice 9 months after secondary transplantation.

**p < 0.01; and ***p < 0.001.

transplantation using WT, *Ezh2*$^{\Delta/\Delta}$, and *Ezh1*$^{+/-}$*Ezh2*$^{\Delta/\Delta}$ BM cells without competitor cells (Figure 2C). Of interest, *Ezh1*$^{+/-}$*Ezh2*$^{\Delta/\Delta}$ BM cells did not engraft in 4 of 10 secondary recipients (Figure 2D) and showed inefficient engraftment in the remaining 6 recipients, although they eventually established high chimerism comparable to that of WT and *Ezh2*$^{\Delta/\Delta}$ cells 6 months after the secondary transplantation (Figure 2E). A genomic PCR of LK cells obtained 9 months after the secondary transplantation revealed the complete deletion of *Ezh2*, ruling out that incompletely excised *Ezh2* in HSCs contributed to the recovery of chimerism (Figure 2F). These results indicate that HSC function was attenuated but still maintained in *Ezh1*$^{+/-}$*Ezh2*$^{\Delta/\Delta}$ mice.

Ezh1 Preferentially Targets Developmental Regulator Genes in *Ezh2*-Insufficient HSPCs

Irrespective of the global loss of H3K27me3, *Ezh1*$^{+/-}$*Ezh2*$^{\Delta/\Delta}$ mice maintained HSC function (Figure 2), whereas DKO mice showed the depletion of HSCs without developing any disease (Figure 2) (Mochizuki-Kashio et al., 2015). These results indicate that the residual H3K27me3 marks mediated by only one allele of *Ezh1* in *Ezh1*$^{+/-}$*Ezh2*$^{\Delta/\Delta}$ mice maintained repression of critical PRC2 TG in HSCs as well as MDS stem cells. To characterize the genome-wide distribution of residual H3K27me3, chromatin immunoprecipitation (ChIP) sequencing (ChIP-seq)/DNA sequencing was performed on hematopoietic stem and progenitor cells (HSPCs) purified from WT, *Ezh1*$^{-/-}$, *Ezh2*$^{\Delta/\Delta}$, and *Ezh1*$^{+/-}$*Ezh2*$^{\Delta/\Delta}$ mice. The enrichment of H3K27me3 ChIP signals over input signals at the promoter region (transcription start site [TSS] $\pm$ 2.0 kb) of each RefSeq gene is shown in scatterplots (Figure 3A). We defined 5,701 genes with H3K27me3 ChIP signals >2-fold over input signals at the promoter region (TSS $\pm$ 2.0 kb) in WT cells as PRC2 TG (Figure 3B and Table S1). The *Ezh1* deletion had a limited effect on H3K27me3 levels, whereas the levels were markedly lower in *Ezh2*$^{\Delta/\Delta}$ and *Ezh1*$^{+/-}$*Ezh2*$^{\Delta/\Delta}$ cells than in WT cells, as expected from western blot data (Figure 1D). Only 970 genes were marked with residual H3K27me3 in *Ezh1*$^{+/-}$*Ezh2*$^{\Delta/\Delta}$ cells, and we defined them as "Ezh1 core target genes" (Ezh1 core TG) (Figure 3B and Table S1). H3K27me3 levels at the promoter regions of Ezh1 core TG were significantly higher than those of PRC2 TG (Figure 3C) and were significantly lower in *Ezh1*$^{-/-}$ and *Ezh1*$^{+/-}$*Ezh2*$^{\Delta/\Delta}$ cells (Figure 3C). However, Ezh1 core TG retained high levels of H3K27me3 mark, even in *Ezh1*$^{-/-}$ cells (Figure 3C), suggesting that they are regulated not only by Ezh1 but also by Ezh2. The majority of H3K27me3 genes in *Ezh1*$^{+/-}$*Ezh2*$^{\Delta/\Delta}$ cells (Ezh1 core TG) were also included in those in WT, *Ezh1*$^{-/-}$, and *Ezh2*$^{\Delta/\Delta}$ cells (Figure 3D). A heatmap clearly showed that the levels of H3K27me3 around the TSS were profoundly lower in *Ezh2*$^{\Delta/\Delta}$ and *Ezh1*$^{+/-}$*Ezh2*$^{\Delta/\Delta}$ cells than in WT and *Ezh1*$^{-/-}$ cells (Figure 3E). These results suggest that in the setting of a PRC2 insufficiency, residual PRC2 is distributed to a restricted number of TG to maintain HSC functions. A gene ontology (GO) analysis showed that Ezh1 core TG were remarkably enriched in genes involved in development, cell differentiation, and transcription (Figure 4A). A total of 37.7% of the Ezh1 core TG were transcription factors or DNA-binding proteins (Figure 4B). The expression of Ezh1 core TG was more tightly repressed in the LSK HSPCs of all genotypes than in PRC2 TG (Figure 4C). Collectively, these results suggest that residual PRC2 preferentially targets developmental regulator genes in *Ezh2*-insufficient HSPCs.

Compared with *Ezh2*$^{\Delta/\Delta}$ LSK cells, *Ezh1*$^{+/-}$*Ezh2*$^{\Delta/\Delta}$ LSK cells lost H3K27me3 at the promoters of 1,035 genes (designated as *Ezh2*$^{\Delta/\Delta}$/*Ezh1*$^{+/-}$*Ezh2*$^{\Delta/\Delta}$ loss genes) (Table S1). A GO analysis showed that these genes were also significantly enriched for developmental regulator genes, despite the much lower levels of enrichment compared with Ezh1core TG (Figure S1A, compared with Figure 4A). Initial levels of H3K27me3 around TSS were higher than those of PRC2 TG, but lower than those of Ezh1 core TG (Figure S1B). Their expression levels were moderately, albeit not significantly, increased in *Ezh1*$^{+/-}$*Ezh2*$^{\Delta/\Delta}$ cells compared with *Ezh2*$^{\Delta/\Delta}$ cells (Figure S1C).

De-repression of Ezh1 Core TG Restricts the Proliferative Capacity of HSCs

To examine the impact of the complete loss of PRC2 on the expression of Ezh1 core TG, we performed RNA sequence analysis on DKO LSK cells. DKO LSK cells were purified from DKO mice 1 week after the deletion of *Ezh2* due to the immediate depletion of HSCs. The complete deletion of *Ezh1* and *Ezh2* in DKO LSK cells, which was confirmed by RNA sequence data (Figure S2A), induced the de-repression of PRC2 TG, including Ezh1 core TG (Figure 5A). To identify the PRC2 TG critical for HSC maintenance, we focused on 42 Ezh1 core TG de-repressed in DKO cells relative to *Ezh1*$^{+/-}$*Ezh2*$^{\Delta/\Delta}$ cells (Figure 5B). Among them, *Cdkn2a*, *Cdkn2b*, *Pitx1* (Liu and Lobie, 2007), *Egr2* (Unoki and Nakamura, 2003), *Egr3* (Cheng et al., 2015), *Tbx15* (Yuan et al., 2011), and *HtrA1* (Supanji et al., 2013) have been reported to negatively regulate cell proliferation or induce cell death. The de-repression of *Cdkn2a*, *Pitx1*, *Egr2*, *Egr3*, *Tbx15*, and *HtrA* in DKO cells was confirmed by a

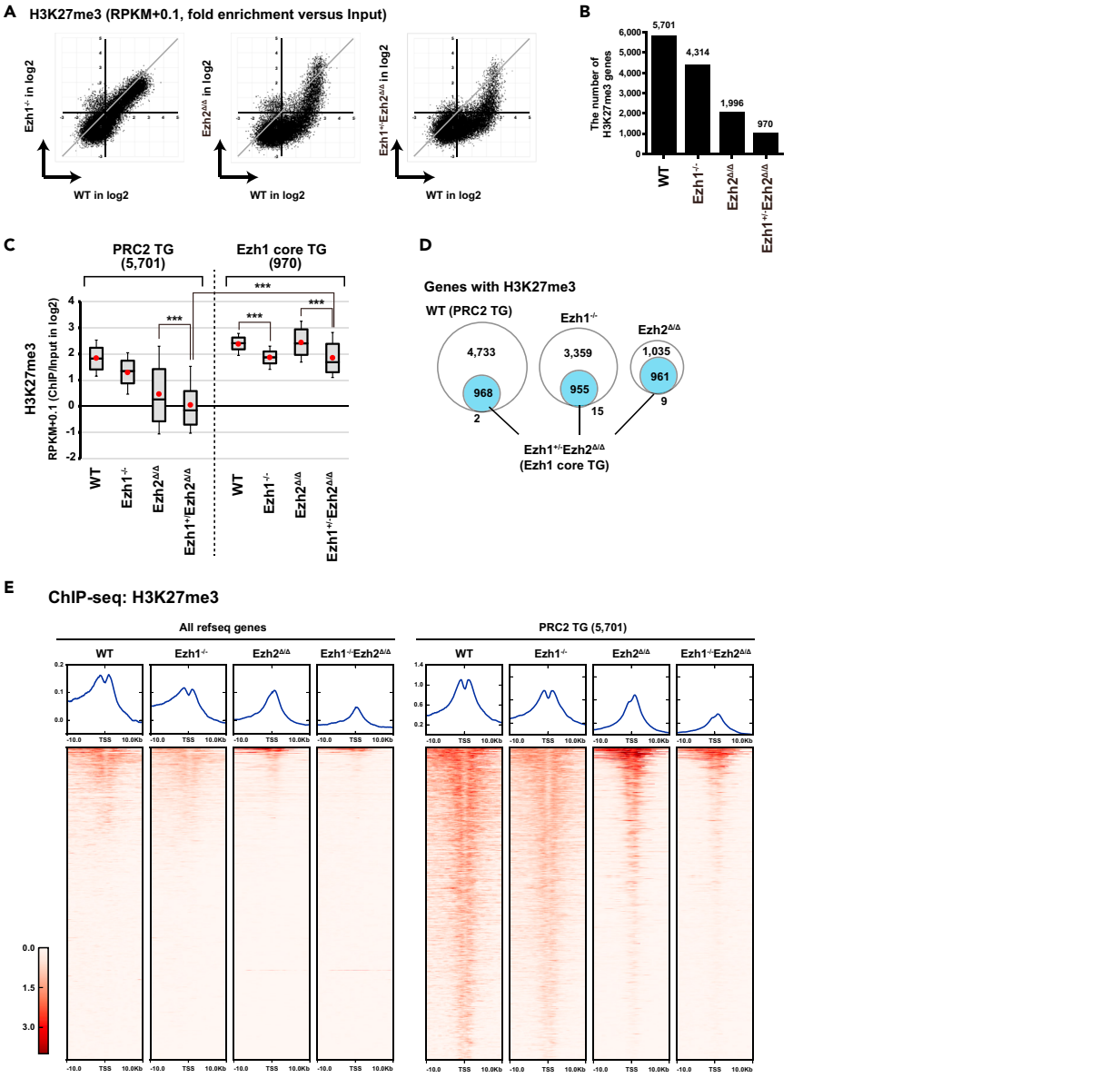

Figure 3. Profiling of PRC2 Target Genes in *Ezh1*$^{+/-}$*Ezh2*$^{\Delta/\Delta}$ HSPCs

(A) Scatterplots showing the relationship of the fold enrichment values of H3K27me3 ChIP signals against the input signals (ChIP/input) at TSS ± 2.0 kb of RefSeq genes (listed in RefSeq ID) between WT and *Ezh1*$^{-/-}$, *Ezh2*$^{\Delta/\Delta}$, or *Ezh1*$^{+/-}$*Ezh2*$^{\Delta/\Delta}$ LK cells 3 months after the tamoxifen treatment.

(B) Bar graph showing the number of H3K27me3 genes that showed ≥ 2-fold enrichment in the level of H3K27me3.

(C) Box-and-whisker plots showing the H3K27me3 levels of PRC2 target genes (TG) and Ezh1 core TG in the indicated mice. Boxes represent 25–75 percentile ranges. Vertical lines represent 10–90 percentile ranges. Horizontal bars represent medians. Mean values are indicated by red dots.

(D) Venn diagram showing the overlap between H3K27me3 genes in *Ezh1*$^{+/-}$*Ezh2*$^{\Delta/\Delta}$ LSK cells (Ezh1 core TG) and those in WT, *Ezh1*$^{-/-}$, or *Ezh2*$^{\Delta/\Delta}$ LSK cells.

(E) Heatmap showing the levels of H3K27me3 at the range of TSS ± 10.0 kb.

quantitative RT-PCR analysis (Figure 5C). Manual ChIP assays also confirmed that H3K27me3 levels were significantly reduced at the promoter of *Cdkn2a*, *Pitx1*, and *Egr3* in DKO cells but kept at high levels in *Ezh1*$^{+/-}$*Ezh2*$^{\Delta/\Delta}$ cells (Figure S2B). *Cdkn2a* and *Cdkn2b* are representative targets of PRC1 and PRC2 that are critical for the maintenance of the proliferative capacity of HSCs (Hidalgo et al., 2012; Oguro et al.,

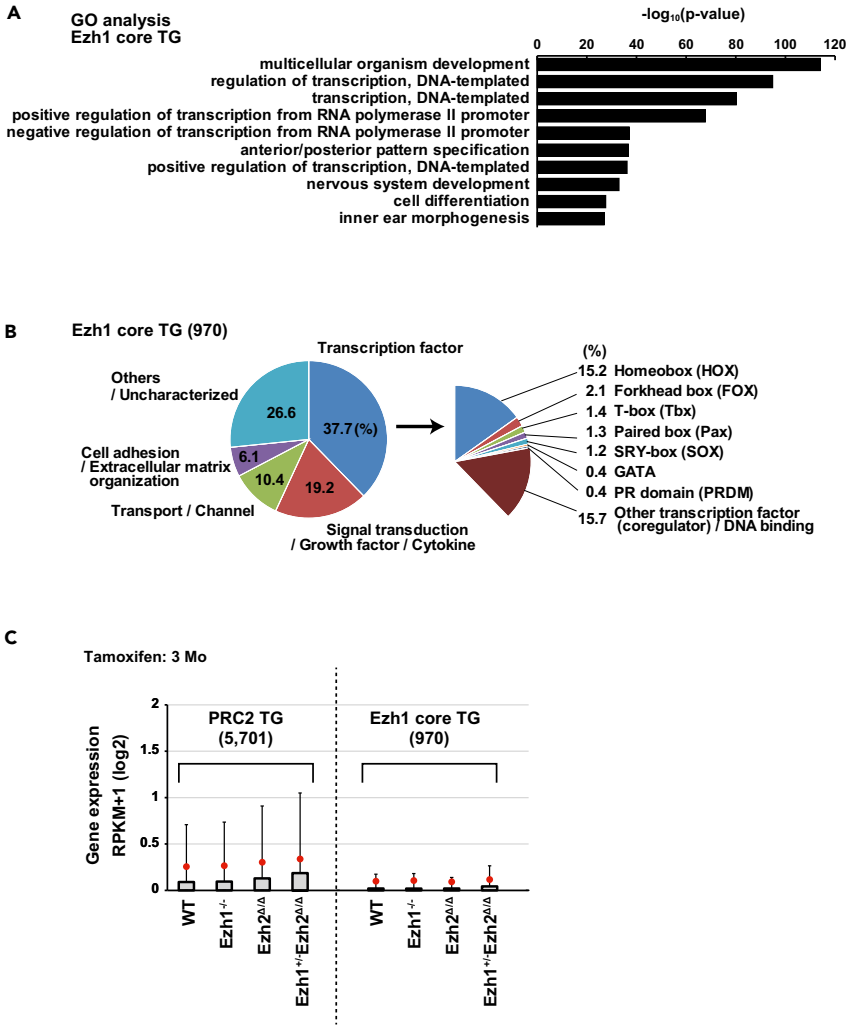

Figure 4. Characterization of Ezh1 Core Target Genes

(A) Gene ontology (GO) analysis of Ezh1 core TG using DAVID Bioinformatics Resources.

(B) Pie graph showing the breakdown of Ezh1 core TG.

(C) Box-and-whisker plots showing the expression levels of PRC2 TG and Ezh1 core TG in LSK cells 3 months (Mo) after the tamoxifen treatment. Boxes represent 25–75 percentile ranges. Vertical lines represent 10–90 percentile ranges. Horizontal bars represent medians. Mean values are indicated by red dots.

2006; Park et al., 2003; Xie et al., 2014). To investigate the effects of the de-repression of other Ezh1 core TG in HSCs and MDS stem cells, we transduced LSK cells with *Pitx1*, *Egr2*, *Egr3*, or *Tbx15* lentiviruses. We purified transduced cells expressing Venus as a marker protein of transduction, and then monitored their growth. A quantitative RT-PCR analysis confirmed a significant overexpression of *Pitx1*, *Egr2*, and *Egr3* (Figure 5D). The overexpression of all the tested genes, particularly *Egr2*, *Egr3*, and *Tbx15*, significantly attenuated the growth of LSK cells under a stem cell culture condition supplemented with Stem cell factor (SCF) and Thrombopoietin (TPO), suggesting that de-repression of each tested gene impairs HSC function (Figure 5E). De-repression of these Ezh1 core TG might account for the exhaustion of HSCs in DKO mice.

H3K4me3 Was Associated with Ezh1 Core TG

Bivalent genes marked with a repressive mark H3K27me3 and an active mark H3K4me3 are the so-called developmental regulator genes that are involved in the regulation of development and differentiation (Bernstein et al., 2006; Zaidi et al., 2017). Given that Ezh1 core TG are rich in developmental regulator genes (Figure 4A), we profiled H3K4me3 in WT and PRC2-insufficient LSK HSPCs by ChIP-seq analysis

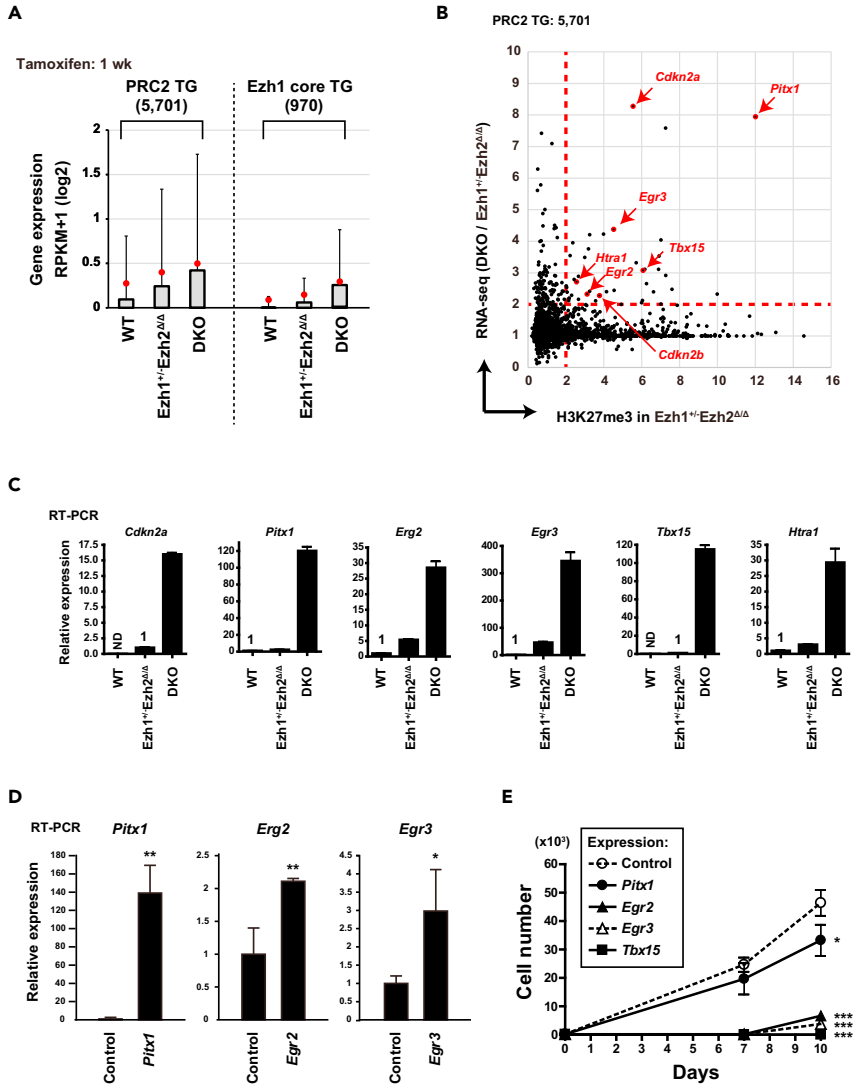

Figure 5. Identification of Responsible Genes Involved in HSC Depletion in PRC2-Null Mice

(A) Box-and-whisker plots showing the expression levels of PRC2 TG and Ezh1 core TG in LSK cells 1 week (wk) after the tamoxifen treatment. Boxes represent 25–75 percentile ranges. Vertical lines represent 10–90 percentile ranges. Horizontal bars represent medians. Mean values are indicated by red dots.

(B) Scatterplots showing the relationship between H3K27me3 levels in *Ezh1*$^{+/-}$*Ezh2*$^{\Delta/\Delta}$ LSK cells and fold expression levels of PRC2 TG in DKO relative to *Ezh1*$^{+/-}$*Ezh2*$^{\Delta/\Delta}$ LSK cells.

(C) A quantitative RT-PCR analysis in WT, *Ezh1*$^{-/-}$*Ezh2*$^{\Delta/\Delta}$, and DKO LSK cells 1 week after the tamoxifen treatment. mRNA levels were normalized to *Hprt1* expression, and relative expression levels are shown as the mean ± SD of triplicate analyses. Cells with expression levels arbitrarily set to 1 are indicated as "1." ND, not detected.

(D and E) Overexpression of selected Ezh1 core TG in WT LSK cells using a lentivirus. Sorted Venus-positive cells were cultured in the presence of SCF and TPO. (D) A quantitative RT-PCR analysis on cells cultured for 10 days. mRNA levels were normalized to *Hprt1* expression, and expression levels relative to the control are shown as the mean ± SD of triplicate analyses. (E) Growth of cells overexpressing the indicated genes. Cell numbers are shown as the mean ± SD of triplicate cultures.

*p < 0.05; **p < 0.01; ***p < 0.001.

(Figure 6A). Genes with both H3K27me3 and H3K4me3 ChIP signals >2-fold over input signals at the promoter region (TSS ± 2.0 kb) in WT cells were defined as bivalent genes in LSK cells. We found that 882 of 970 Ezh1 core TG were overlapped with the bivalent genes (Figure 6B) and were significantly enriched for developmental regulator genes, as evident from the data of GO analysis (Figure 6C). A heatmap and the

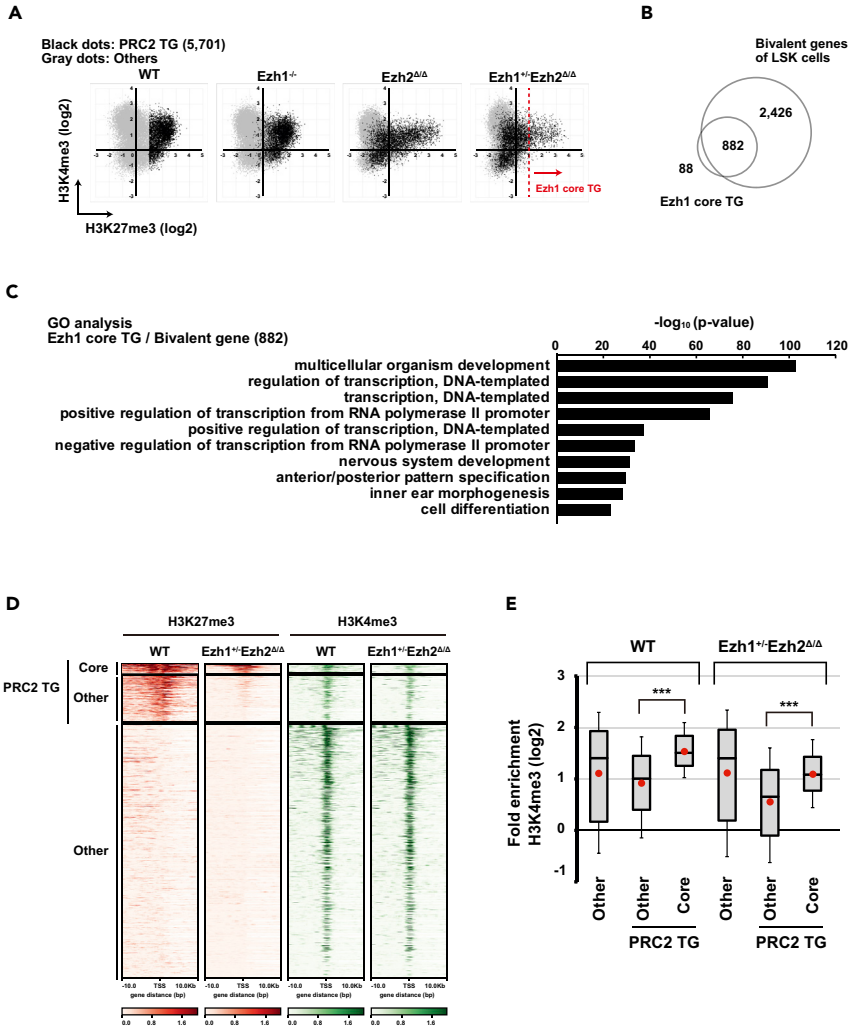

Figure 6. Profiling of H3K4me3 in *Ezh1*$^{+/-}$*Ezh2*$^{\Delta/\Delta}$ HSPCs

(A) Scatterplots showing the relationship of the fold enrichment values (ChIP/input) of H3K27me3 and H3K4me3 at TSS ± 2.0 kb of RefSeq genes. WT, *Ezh1*$^{-/-}$, *Ezh2*$^{\Delta/\Delta}$, and *Ezh1*$^{+/-}$*Ezh2*$^{\Delta/\Delta}$ LSK cells were obtained from mice 3 months after the tamoxifen treatment. Black and gray dots indicate PRC2 TG and others, respectively.

(B) Venn diagram showing the overlap between Ezh1 core TG and bivalent genes in WT LSK cells.

(C) GO analysis data of Ezh1 core TG overlapping with bivalent genes in (B) using DAVID Bioinformatics Resources.

(D) Heatmap showing H3K27me3 and H3K4me3 levels at the range of TSS ± 10.0 kb.

(E) Box-and-whisker plots showing H3K4me3 levels. Boxes represent 25–75 percentile ranges. Vertical lines represent 10–90 percentile ranges. Horizontal bars represent medians. Mean values are indicated by red dots. ***$p < 0.001$.

following quantitative analysis showed that the levels of H3K4me3 at the promoters of Ezh1 core TG were remarkably higher than those at other PRC2 TG in both WT and *Ezh1*$^{+/-}$*Ezh2*$^{\Delta/\Delta}$ cells (Figures 6D and 6E). Levels of H3K4me3 at the promoters of Ezh1 core TG were slightly reduced in *Ezh1*$^{+/-}$*Ezh2*$^{\Delta/\Delta}$ cells but stayed at higher levels than those at other PRC2 TG (Figures 6A, 6D, and 6E). Taken together, these data suggest that residual PRC2 preferentially targets bivalent developmental regulator genes in its insufficiency.

PRC1-Mediated H2AK119ub1 Was Involved in Repression of Ezh1 Core TG

PRC1 largely shares TG with PRC2 because PRC1-mediated H2AK119ub1 functions up- and downstream of PRC2-mediated H3K27me3 (Blackledge et al., 2014, 2015; Cooper et al., 2016; Kalb et al., 2014). We hypothesized that H2AK119ub1 also plays a key role in the repression of PRC2 TG in PRC2-insufficient HSPCs. To test this hypothesis, the state of the H2AK119ub1 modification in *Ezh1*$^{+/-}$*Ezh2*$^{\Delta/\Delta}$ LSK HSPCs was

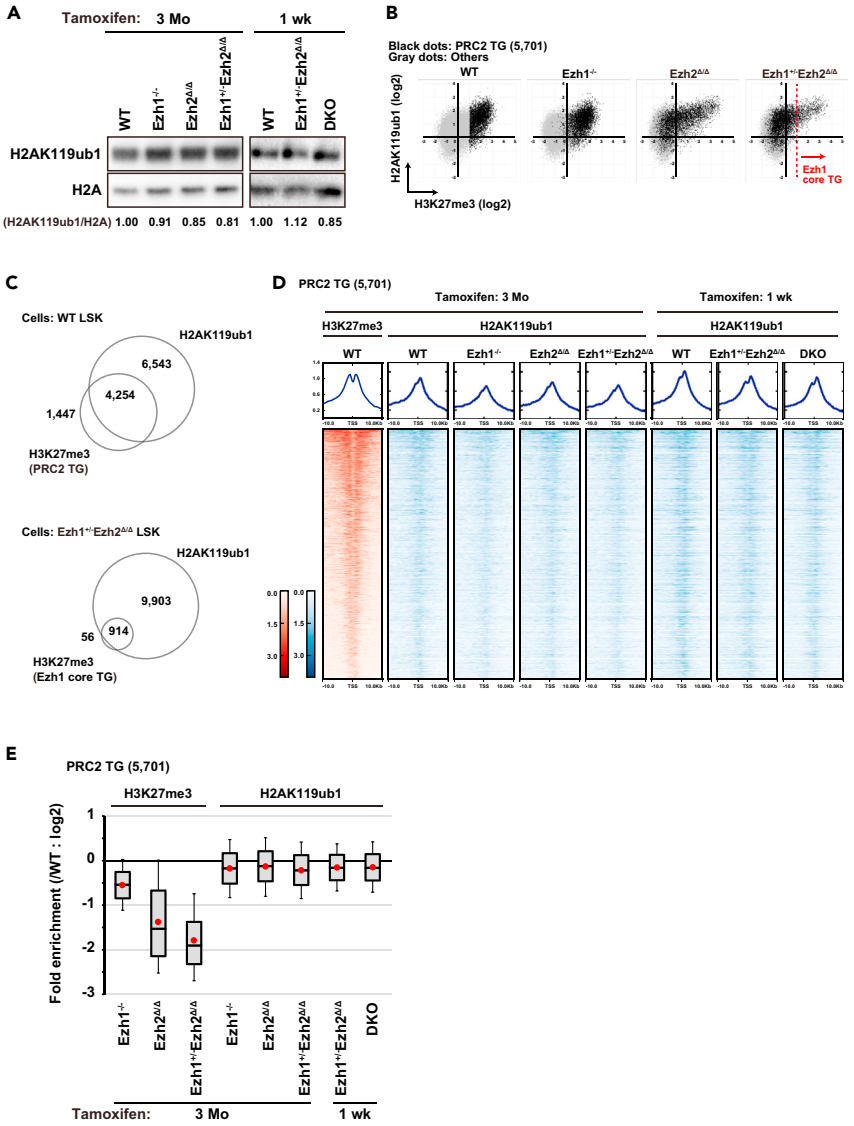

Figure 7. Involvement of H2AK119ub1 in Repression of Ezh1 Core TG

(A) Western blot analysis of global histone modification levels in hematopoietic progenitor cells (HPCs). LK cells obtained from mice 3 months (Mo) or c-Kit$^+$ cells obtained 1 week (wk) after the tamoxifen treatment were subjected to a western blot analysis using anti-H2AK119ub1 and histone H2A antibodies. H2AK119ub1 amounts relative to total H2A are indicated.

(B) Scatterplots showing the relationship of the fold enrichment values (ChIP/input) of H3K27me3 and H2AK119ub1 at TSS ± 2.0 kb of RefSeq genes. WT, *Ezh1*$^{-/-}$, *Ezh2*$^{\Delta/\Delta}$, and *Ezh1*$^{+/-}$*Ezh2*$^{\Delta/\Delta}$ LSK cells were obtained from mice 3 months after the tamoxifen treatment. Black and gray dots indicate PRC2 TG and others, respectively.

(C) Venn diagram showing the overlap between genes marked with H2AK119ub1 and those with H3K27me3 at their promoters in WT (upper) and *Ezh1*$^{+/-}$*Ezh2*$^{\Delta/\Delta}$ (lower) LSK cells.

(D) Heatmap showing H3K27me3 and H2AK119ub1 levels at the range of TSS ±10.0 kb of PRC2 TG in LSK cells 3 months or c-Kit$^+$ cells 1 week after the tamoxifen treatment.

(E) Box-and-whisker plots showing H3K27me3 and H2AK119ub1 levels of PRC2 TG. Boxes represent 25–75 percentile ranges. Vertical lines represent 10–90 percentile ranges. Horizontal bars represent medians. Mean values are indicated by red dots.

examined. For analysis on DKO HSPCs, c-Kit$^+$ BM cells that were collected 1 week after tamoxifen treatment were used. A western blot analysis showed that the global level of H2AK119ub1 was not significantly changed by the loss of PRC2, even in DKO cells (Figure 7A). A ChIP-seq analysis of H2AK119ub1 revealed a

strong correlation of H2AK119ub1 levels with H3K27me3 levels at the promoters of PRC2 TG, particularly of the Ezh1 core TG in *Ezh1*$^{+/-}$*Ezh2*$^{\Delta/\Delta}$ cells (Figure 7B). The genes, the promoters of which were marked with H3K27me3 and H2AK119ub1, largely overlapped (Figure 7C). A heatmap and boxplot showed that the deletion of *Ezh1* and/or *Ezh2* had limited effects on the level of H2AK119ub1 at the promoters of PRC2 TG (Figures 7D and 7E), which is consistent with the global levels of H2AK119ub1 detected in western blots (Figure 7A). Manual ChIP assays confirmed that H2AK119ub1 levels of selected Ezh1 core TG were maintained at the basal levels in DKO as well as *Ezh1*$^{+/-}$*Ezh2*$^{\Delta/\Delta}$ HSPCs (Figure S2C). These results suggest a role for PRC1-mediated H2AK119ub1 in the repression of PRC2 TG in the setting of a PRC2 insufficiency.

DISCUSSION

Only Ezh2 and its paralog Ezh1 function as H3K27 methyltransferases. No other enzymes have been shown to exhibit similar catalytic activities. We previously reported that the hematopoietic-cell-specific deletion of *Ezh2* did not compromise the self-renewal capacity of HSCs and caused heterogeneous hematological malignancies, including MDS, in mice. In contrast, *Ezh1*$^{-/-}$*Ezh2*$^{\Delta/\Delta}$ mice failed to maintain HSCs as well as MDS stem cells (Mochizuki-Kashio et al., 2015). Here, our ChIP-seq analysis provided a new insight into the epigenetic mechanisms of maintenance of HSCs and MDS stem cells in the setting of an *Ezh2* insufficiency.

Another group also reported the requirement of PRC2 for HSC maintenance using *Eed*-deleted mice, which are similar to *Ezh1*$^{-/-}$*Ezh2*$^{\Delta/\Delta}$ (DKO) mice in terms of the complete loss of PRC2 activity (Xie et al., 2014). These findings suggest that Ezh1 plays an important role in the maintenance of HSCs and development of MDS in the setting of an *Ezh2* insufficiency. In the present study, we demonstrated that only one allele of *Ezh1* (*Ezh1*$^{+/-}$*Ezh2*$^{\Delta/\Delta}$) was sufficient to maintain HSCs as well as MDS stem cells (Figure 2), despite the markedly weaker catalytic activity of Ezh1 than Ezh2 (Margueron et al., 2008). This result indicates that the minimal levels of H3K27me3 mediated by Ezh1 are sufficient for HSC maintenance.

The enzymatic activity of Ezh1 was previously shown to be markedly weaker than that of Ezh2 *in vitro* and *in vivo* (Margueron et al., 2008). Correspondingly, the deletion of *Ezh1* alone (*Ezh1*$^{-/-}$) affected H3K27me3 levels in HSPCs much less than that of *Ezh2*. However, in the absence of Ezh2, *Ezh1* heterozygosity had a significant impact on H3K27me3 levels at the promoters of PRC2 TG (Figures 3A–3C and 3E). Only 970 genes retained H3K27me3 at their promoters in *Ezh1*$^{+/-}$*Ezh2*$^{\Delta/\Delta}$ HSPCs (Figure 3B). These 970 genes, defined as "Ezh1 core TG," were strongly enriched in genes coding for transcription factors and developmental regulators (Figures 4A and 4B). The forced expression of selected Ezh1 core TG that were de-repressed in DKO HSPCs, including *Pitx1*, *Egr2*, *Egr3*, and *Tbx15*, suppressed the growth of LSK cells *in vitro* (Figure 5E). Diffuse intrinsic pontine glioma cells with the mutation of H3K27M exhibited attenuated PRC2 function with the global loss of H3K27me3, whereas the H3K27me3 mark was retained by a limited number of genes, including the tumor suppressor gene *CDKN2A*. The inhibition of residual PRC2 activity abolished tumor cell growth following the de-repression of *CDKN2A* (Mohammad et al., 2017). Collectively, these findings indicate that residual PRC2 preferentially targets critical genes for the maintenance of stem cells in PRC2-insufficient tumor cells. In contrast, 1,035 *Ezh2*$^{\Delta/\Delta}$/*Ezh1*$^{+/-}$*Ezh2*$^{\Delta/\Delta}$ loss genes, which lost H3K27me3 at the promoters in *Ezh1*$^{+/-}$*Ezh2*$^{\Delta/\Delta}$ LSK cells compared with *Ezh2*$^{\Delta/\Delta}$ LSK cells, also included many developmental regulator genes, and their expression levels were moderately increased in *Ezh1*$^{+/-}$*Ezh2*$^{\Delta/\Delta}$ cells compared with *Ezh2*$^{\Delta/\Delta}$ cells (Figures S1A–S1C). Given that the de-repression of developmental regulator genes of Ezh1 core targets affect the function of HSCs, de-repression of *Ezh2*$^{\Delta/\Delta}$/*Ezh1*$^{+/-}$*Ezh2*$^{\Delta/\Delta}$ loss genes also could account for the defective function of *Ezh1*$^{+/-}$*Ezh2*$^{\Delta/\Delta}$ HSCs/MDS stem cells as observed in Figure 2.

In addition to H3K27me3, we profiled H3K4me3 in PRC2-insufficient HSPCs (Figure 6A), since the bivalency of these histone modifications are frequently observed at the promoters of developmental regulator genes (Bernstein et al., 2006; Ku et al., 2008; Zaidi et al., 2017). Consistent with the results of GO analysis (Figure 4A), Ezh1 core TG were mostly bivalent genes in LSK cells (Figure 6B). Of note, we detected remarkably higher levels of H3K4me3 at Ezh1 core TG than other PRC2 TG (Figures 6D and 6E). The high levels of H3K4me3 could serve as a marker for selective targeting of residual PRC2 to Ezh1 core TG.

Many of the developmental regulator genes, such as *Hox* genes, which are well-known targets of PRC2, were included in Ezh1 core TG, but continued to be repressed in PRC2-insufficient LSK cells, even in DKO mice (Figures 4C, 5A, and 5B). They appeared to be repressed by mechanisms other than PRC2-mediated H3K27me3 in HSPCs. H2AK119ub1 cooperates with H3K27me3 to form a repressive chromatin region called the polycomb domain. In the traditional model, PRC1, which catalyzes H2AK119ub1, is recruited to PRC2-mediated H3K27me3. However, recent studies reported an alternative mechanism, in which PRC1 deposits H2AK119ub1 independently of PRC2. This new type of PRC1 complex has been classified as variant PRC1, whereas PRC1 in the traditional model is called canonical PRC1 (Blackledge et al., 2015). H2AK119ub1 levels were previously shown to be largely retained in PRC2-deficient mouse ES cells (Tavares et al., 2012). Consistent with this finding, we demonstrated that DKO HSPCs exhibited almost the complete retention of H2AK119ub1 at the global level as well as at the promoters of PRC2 TG, suggesting that variant PRC1s, but not canonical PRC1, predominantly contribute to the deposition of H2AK119ub1 in HSPCs as well as in mouse ES cells (Figures 7A, 7D, and 7E). Since variant PRC1-mediated H2AK119ub1 recruits PRC2, leading to the deposition of H3K27me3 (Blackledge et al., 2014), variant PRC1-mediated H2AK119ub1 may be one of the mechanisms underlying the preferential targeting of PRC2 to Ezh1 core TG, as well as H3K4me3. In fact, we found that this mark strongly co-localized with H3K27me3 at Ezh1 core TG in $Ezh1^{+/-}Ezh2^{\Delta/\Delta}$ HSPCs (Figure 7B). Intriguingly, inhibition of Ring1A, an enzymatic component of PRC1, has been shown to have an antitumor effect on an MDS cell line and primary $CD34^{+}$ cells from patients with MDS (Palau et al., 2017). Therefore, the functional inhibition of PRC1, especially variant PRC1, would represent an interesting approach to eradicate MDS stem cells by inducing the de-repression of Ezh1 core TG in *Ezh2*-insufficient MDS.

METHODS

All methods can be found in the accompanying Transparent Methods supplemental file.

SUPPLEMENTAL INFORMATION

Supplemental Information includes Transparent Methods, two figures, and one table and can be found with this article online at https://doi.org/10.1016/j.isci.2018.10.008.

ACKNOWLEDGMENTS

Ezh1 constitutive knockout mice were generated at the Research Institute of Molecular Pathology (Vienna, Austria) in 2000 by Donal O'Carroll (Laboratory Thomas Jenuwein) with the help of Maria Sibilia (Laboratory Erwin Wagner). $Ezh2^{fl/fl}$ mice were kindly provided by Haruhiko Koseki (RIKEN, Japan). The authors thank Yuko Yamagata for her technical help. The supercomputing resource was provided by the Human Genome Center, Institute of Medical Science, University of Tokyo. This work was supported in part by Grants-in-Aid for Scientific Research (#15H02544) and Scientific Research on Innovative Areas "Stem Cell Aging and Disease" (#25115002) from MEXT, Japan, and grants from the Naito Foundation and Takamatsunomiya Princess Cancer Research Fund.

AUTHOR CONTRIBUTIONS

K.A. performed the experiments, analyzed results, made the figures, and actively wrote the manuscript; M.O., S.K., E.S., M.M.-K., Y.K., S.T., D.S., N.H., Y.N.-T., and G.S. assisted with the experiments; and A.I. conceived of and directed the project, secured funding, and actively wrote the manuscript.

DECLARATION OF INTERESTS

The authors have no competing financial interests to declare.

Received: July 3, 2018
Revised: October 9, 2018
Accepted: October 9, 2018
Published: November 30, 2018

REFERENCES

Bernstein, B.E., Mikkelsen, T.S., Xie, X., Kamal, M., Huebert, D.J., Cuff, J., Fry, B., Meissner, A., Wernig, M., Plath, K., et al. (2006). A bivalent chromatin structure marks key developmental genes in embryonic stem cells. Cell *125*, 315–326.

Blackledge, N.P., Farcas, A.M., Kondo, T., King, H.W., McGouran, J.F., Hanssen, L.L., Ito, S., Cooper, S., Kondo, K., Koseki, Y., et al. (2014). Variant PRC1 complex-dependent H2A ubiquitylation drives PRC2 recruitment and polycomb domain formation. Cell *157*, 1445–1459.

Blackledge, N.P., Rose, N.R., and Klose, R.J. (2015). Targeting Polycomb systems to regulate gene expression: modifications to a complex story. Nat. Rev. Mol. Cell Biol. *16*, 643–649.

Cheng, H., Hao, S., Liu, Y., Pang, Y., Ma, S., Dong, F., Xu, J., Zheng, G., Li, S., Yuan, W., et al. (2015). Leukemic marrow infiltration reveals a novel role for Egr3 as a potent inhibitor of normal hematopoietic stem cell proliferation. Blood *126*, 1302–1313.

Conway, E., Healy, E., and Bracken, A.P. (2015). PRC2 mediated H3K27 methylations in cellular identity and cancer. Curr. Opin. Cell Biol. *37*, 42–48.

Cooper, S., Grijzenhout, A., Underwood, E., Ancelin, K., Zhang, T., Nesterova, T.B., Anil-Kirmizitas, B., Bassett, A., Kooistra, S.M., Agger, K., et al. (2016). Jarid2 binds mono-ubiquitylated H2A lysine 119 to mediate crosstalk between Polycomb complexes PRC1 and PRC2. Nat. Commun. *7*, 13661.

Ezhkova, E., Lien, W.H., Stokes, N., Pasolli, H.A., Silva, J.M., and Fuchs, E. (2011). EZH1 and EZH2 cogovern histone H3K27 trimethylation and are essential for hair follicle homeostasis and wound repair. Genes Dev. *25*, 485–498.

Henriquez, B., Bustos, F.J., Aguilar, R., Becerra, A., Simon, F., Montecino, M., and van Zundert, B. (2013). Ezh1 and Ezh2 differentially regulate PSD-95 gene transcription in developing hippocampal neurons. Mol. Cell. Neurosci. *57*, 130–143.

Hidalgo, I., Herrera-Merchan, A., Ligos, J.M., Carramolino, L., Nunez, J., Martinez, F., Dominguez, O., Torres, M., and Gonzalez, S. (2012). Ezh1 is required for hematopoietic stem cell maintenance and prevents senescence-like cell cycle arrest. Cell Stem Cell *11*, 649–662.

Holoch, D., and Margueron, R. (2017). Mechanisms regulating PRC2 recruitment and enzymatic activity. Trends Biochem. Sci. *42*, 531–542.

Honda, H., Nagamachi, A., and Inaba, T. (2015). -7/7q- syndrome in myeloid-lineage hematopoietic malignancies: attempts to understand this complex disease entity. Oncogene *34*, 2413–2425.

Iwama, A. (2017). Polycomb repressive complexes in hematological malignancies. Blood *130*, 23–29.

Kalb, R., Latwiel, S., Baymaz, H.I., Jansen, P.W., Muller, C.W., Vermeulen, M., and Muller, J. (2014). Histone H2A monoubiquitination promotes histone H3 methylation in Polycomb repression. Nat. Struct. Mol. Biol. *21*, 569–571.

Kondo, T., Ito, S., and Koseki, H. (2016). Polycomb in transcriptional phase transition of developmental genes. Trends Biochem. Sci. *41*, 9–19.

Ku, M., Koche, R.P., Rheinbay, E., Mendenhall, E.M., Endoh, M., Mikkelsen, T.S., Presser, A., Nusbaum, C., Xie, X., Chi, A.S., et al. (2008). Genomewide analysis of PRC1 and PRC2 occupancy identifies two classes of bivalent domains. PLoS Genet. *4*, e1000242.

Liu, D.X., and Lobie, P.E. (2007). Transcriptional activation of p53 by Pitx1. Cell Death Differ. *14*, 1893–1907.

Margueron, R., Li, G., Sarma, K., Blais, A., Zavadil, J., Woodcock, C.L., Dynlacht, B.D., and Reinberg, D. (2008). Ezh1 and Ezh2 maintain repressive chromatin through different mechanisms. Mol. Cell *32*, 503–518.

Margueron, R., and Reinberg, D. (2011). The Polycomb complex PRC2 and its mark in life. Nature *469*, 343–349.

Mochizuki-Kashio, M., Aoyama, K., Sashida, G., Oshima, M., Tomioka, T., Muto, T., Wang, C., and Iwama, A. (2015). Ezh2 loss in hematopoietic stem cells predisposes mice to develop heterogeneous malignancies in an Ezh1-dependent manner. Blood *126*, 1172–1183.

Mohammad, F., Weissmann, S., Leblanc, B., Pandey, D.P., Hojfeldt, J.W., Comet, I., Zheng, C., Johansen, J.V., Rapin, N., Porse, B.T., et al. (2017). EZH2 is a potential therapeutic target for H3K27M-mutant pediatric gliomas. Nat. Med. *23*, 483–492.

Morin, R.D., Johnson, N.A., Severson, T.M., Mungall, A.J., An, J., Goya, R., Paul, J.E., Boyle, M., Woolcock, B.W., Kuchenbauer, F., et al. (2010). Somatic mutations altering EZH2 (Tyr641) in follicular and diffuse large B-cell lymphomas of germinal-center origin. Nat. Genet. *42*, 181–185.

Mousavi, K., Zare, H., Wang, A.H., and Sartorelli, V. (2012). Polycomb protein Ezh1 promotes RNA polymerase II elongation. Mol. Cell *45*, 255–262.

Muto, T., Sashida, G., Oshima, M., Wendt, G.R., Mochizuki-Kashio, M., Nagata, Y., Sanada, M., Miyagi, S., Saraya, A., Kamio, A., et al. (2013). Concurrent loss of Ezh2 and Tet2 cooperates in the pathogenesis of myelodysplastic disorders. J. Exp. Med. *210*, 2627–2639.

Oguro, H., Iwama, A., Morita, Y., Kamijo, T., van Lohuizen, M., and Nakauchi, H. (2006). Differential impact of Ink4a and Arf on hematopoietic stem cells and their bone marrow microenvironment in Bmi1-deficient mice. J. Exp. Med. *203*, 2247–2253.

Palau, A., Garz, A.K., Diesch, J., Zwick, A., Malinverni, R., Valero, V., Lappin, K., Casquero, R., Lennartsson, A., Zuber, J., et al. (2017). Polycomb protein RING1A limits hematopoietic differentiation in myelodysplastic syndromes. Oncotarget *8*, 115002–115017.

Park, I.K., Qian, D., Kiel, M., Becker, M.W., Pihalja, M., Weissman, I.L., Morrison, S.J., and Clarke, M.F. (2003). Bmi-1 is required for maintenance of adult self-renewing haematopoietic stem cells. Nature *423*, 302–305.

Pasini, D., Malatesta, M., Jung, H.R., Walfridsson, J., Willer, A., Olsson, L., Skotte, J., Wutz, A., Porse, B., Jensen, O.N., et al. (2010). Characterization of an antagonistic switch between histone H3 lysine 27 methylation and acetylation in the transcriptional regulation of Polycomb group target genes. Nucleic Acids Res. *38*, 4958–4969.

Sashida, G., Harada, H., Matsui, H., Oshima, M., Yui, M., Harada, Y., Tanaka, S., Mochizuki-Kashio, M., Wang, C., Saraya, A., et al. (2014). Ezh2 loss promotes development of myelodysplastic syndrome but attenuates its predisposition to leukaemic transformation. Nat. Commun. *5*, 4177.

Sashida, G., and Iwama, A. (2017). Multifaceted role of the polycomb-group gene EZH2 in hematological malignancies. Int. J. Hematol. *105*, 23–30.

Sashida, G., Wang, C., Tomioka, T., Oshima, M., Aoyama, K., Kanai, A., Mochizuki-Kashio, M., Harada, H., Shimoda, K., and Iwama, A. (2016). The loss of Ezh2 drives the pathogenesis of myelofibrosis and sensitizes tumor-initiating cells to bromodomain inhibition. J. Exp. Med. *213*, 1459–1477.

Shen, X., Liu, Y., Hsu, Y.J., Fujiwara, Y., Kim, J., Mao, X., Yuan, G.C., and Orkin, S.H. (2008). EZH1 mediates methylation on histone H3 lysine 27 and complements EZH2 in maintaining stem cell identity and executing pluripotency. Mol. Cell *32*, 491–502.

Stojic, L., Jasencakova, Z., Prezioso, C., Stutzer, A., Bodega, B., Pasini, D., Klingberg, R., Mozzetta, C., Margueron, R., Puri, P.L., et al. (2011). Chromatin regulated interchange between polycomb repressive complex 2 (PRC2)-Ezh2 and PRC2-Ezh1 complexes controls myogenin activation in skeletal muscle cells. Epigenetics Chromatin *4*, 16.

Supanji, Shimomachi, M., Hasan, M.Z., Kawaichi, M., and Oka, C. (2013). HtrA1 is induced by oxidative stress and enhances cell senescence through p38 MAPK pathway. Exp. Eye Res. *112*, 79–92.

Tavares, L., Dimitrova, E., Oxley, D., Webster, J., Poot, R., Demmers, J., Bezstarosti, K., Taylor, S., Ura, H., Koide, H., et al. (2012). RYBP-PRC1 complexes mediate H2A ubiquitylation at polycomb target sites independently of PRC2 and H3K27me3. Cell *148*, 664–678.

Unoki, M., and Nakamura, Y. (2003). EGR2 induces apoptosis in various cancer cell lines by direct transactivation of BNIP3L and BAK. Oncogene *22*, 2172–2185.

Xie, H., Xu, J., Hsu, J.H., Nguyen, M., Fujiwara, Y., Peng, C., and Orkin, S.H. (2014).

Polycomb repressive complex 2 regulates normal hematopoietic stem cell function in a developmental-stage-specific manner. Cell Stem Cell *14*, 68–80.

Xu, J., Shao, Z., Li, D., Xie, H., Kim, W., Huang, J., Taylor, J.E., Pinello, L., Glass, K., Jaffe, J.D., et al. (2015). Developmental control of polycomb subunit composition by GATA factors mediates a switch to non-canonical functions. Mol. Cell *57*, 304–316.

Yuan, J., Takeuchi, M., Negishi, M., Oguro, H., Ichikawa, H., and Iwama, A. (2011). Bmi1 is essential for leukemic reprogramming of myeloid progenitor cells. Leukemia *25*, 1335–1343.

Zaidi, S.K., Frietze, S.E., Gordon, J.A., Heath, J.L., Messier, T., Hong, D., Boyd, J.R., Kang, M., Imbalzano, A.N., Lian, J.B., et al. (2017). Bivalent epigenetic control of oncofetal gene expression in cancer. Mol. Cell Biol. *37*, e000352–17.

ISCI, Volume *9*

Supplemental Information

Ezh1 Targets Bivalent Genes to Maintain Self-Renewing Stem Cells in *Ezh2*-Insufficient Myelodysplastic Syndrome

Kazumasa Aoyama, Motohiko Oshima, Shuhei Koide, Emi Suzuki, Makiko Mochizuki-Kashio, Yuko Kato, Shiro Tara, Daisuke Shinoda, Nobuhiro Hiura, Yaeko Nakajima-Takagi, Goro Sashida, and Atsushi Iwama

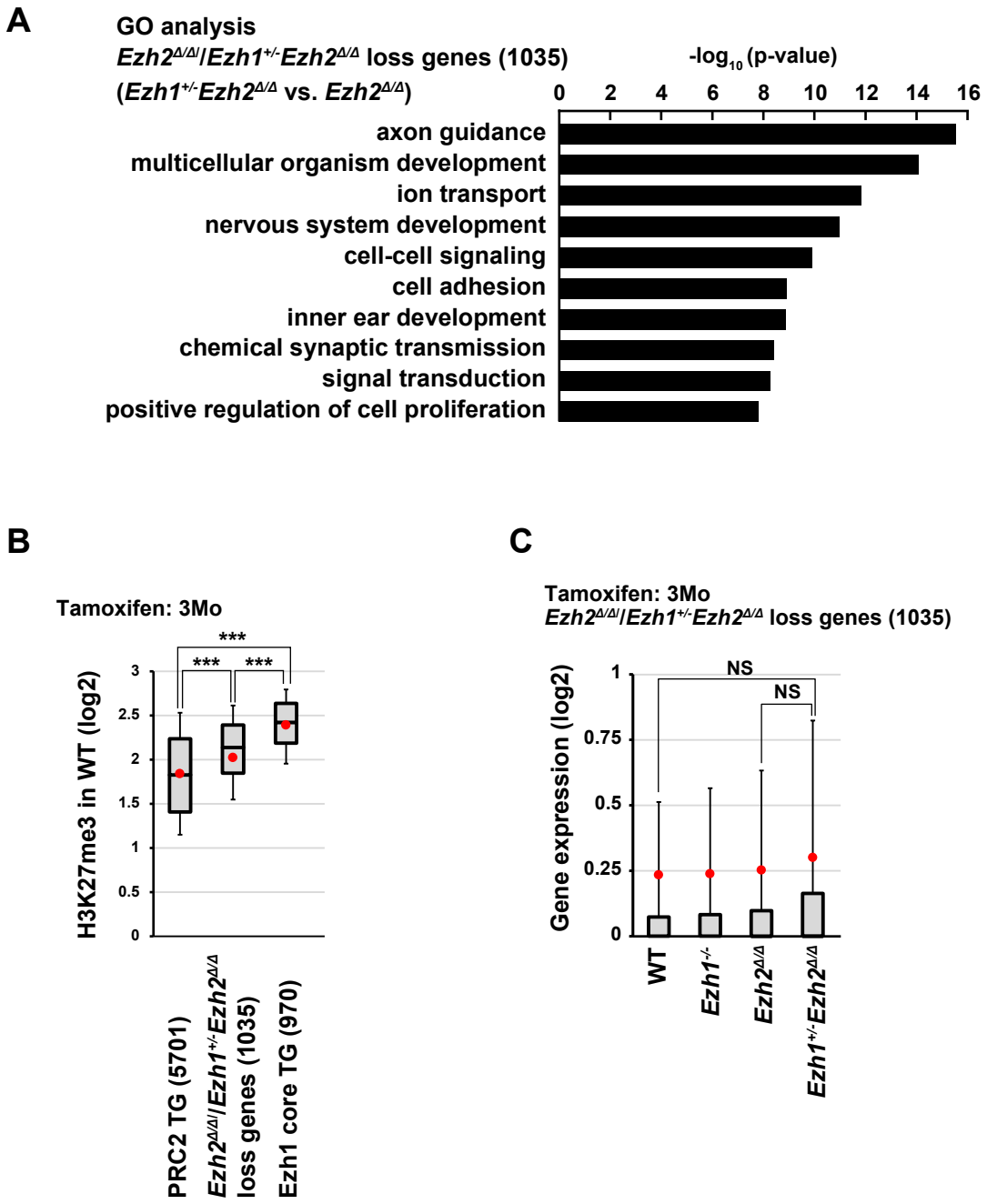

Figure S1 related to Figures 3 and 4.
(A) Gene ontology analysis of 1,035 *Ezh2*$^{\Delta/\Delta/}$*Ezh1*$^{+/-}$*Ezh2*$^{\Delta/\Delta}$ loss genes (1035) using DAVID Bioinformatics Resources.
(B, C) Box-and-whisker plots showing H3K27me3 levels of PRC2 TG, *Ezh2*$^{\Delta/\Delta/}$*Ezh1*$^{+/-}$*Ezh2*$^{\Delta/\Delta}$ loss genes, and Ezh1 core TG in WT LSK cells (B) and the expression levels of *Ezh2*$^{\Delta/\Delta/}$*Ezh1*$^{+/-}$*Ezh2*$^{\Delta/\Delta}$ loss genes in LSK cells 3 months after the tamoxifen treatment (C). Boxes represent 25-75 percentile ranges. Vertical lines represent 10-90 percentile ranges. Horizontal bars represent medians. Mean values are indicated by red dots. ***, p<0.001; NS, Not significant.

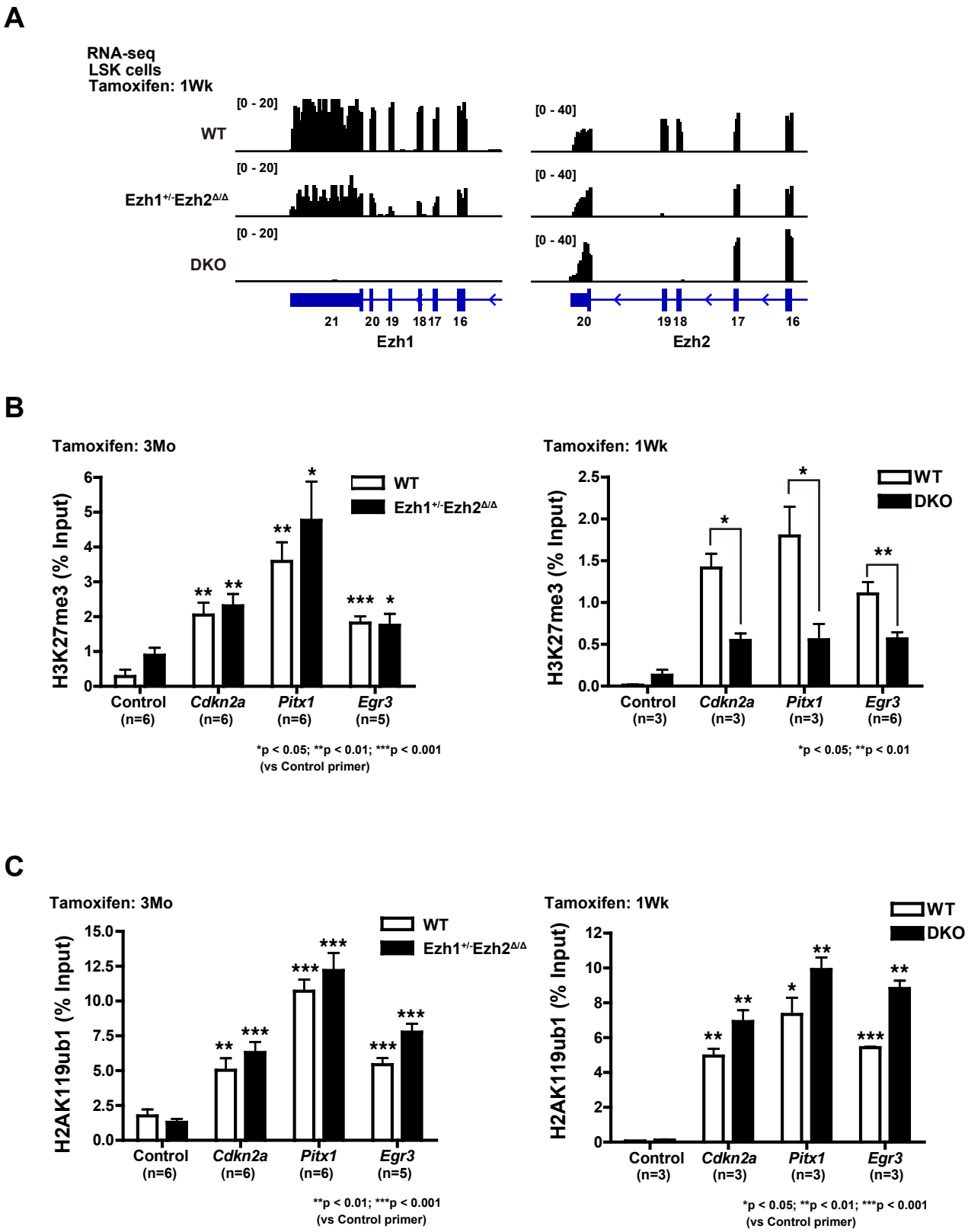

Figure S2 related to Figures 5 and 7.
(A) Snapshots of RNA-seq signals at *Ezh1* and *Ezh2* gene loci in WT, *Ezh1*$^{+/-}$*Ezh2*$^{\Delta/\Delta}$ and DKO LSK cells isolated from recipient mice 1 week after the tamoxifen treatment.
(B, C) Manual ChIP assays for H3K27me3 or H2AK119ub1 at the promoters of *Cdkn2a*, *Pitx1*, and *Egr3*. WT and *Ezh1*$^{+/-}$*Ezh2*$^{\Delta/\Delta}$ LSK cells 3 months after the tamoxifen treatment and WT and DKO c-kit^{+} BM cells 1 week after the tamoxifen treatment were used (left and right panels, respectively). The relative amounts of immunoprecipitated DNA are depicted as a percentage of input DNA. Data are shown as the mean ± SD. The Student's *t*-test was performed compared to a control locus (B, left panel and C). *, p<0.05; **, p<0.01; and ***, p<0.001.

Transparent Methods

Mice

As described previously (Mochizuki-Kashio et al., 2015), *Ezh2*$^{fl/fl}$ mice (Hirabayashi et al., 2009) were crossed with *Rosa26::Cre-ERT* mice (TaconicArtemis GmbH) to achieve the conditional deletion of *Ezh2*. These mice were injected with 100 µl of tamoxifen dissolved in corn oil at a concentration of 10 mg/ml intraperitoneally for 5 consecutive days to induce Cre-ERT activity. *Ezh1* constitutive knockout mice were obtained from Thomas Jenuwein's laboratory and will be reported elsewhere. Some of its phenotypes have been reported previously (Bae et al., 2015; Ezhkova et al., 2011; Mochizuki-Kashio et al., 2015). C57BL/6 mice congenic for the Ly5 locus (CD45.1) were purchased from Sankyo-Lab Service (Tsukuba, Japan). All experiments using mice were performed in accordance with our institutional guidelines for the use of laboratory animals and approved by the Review Board for Animal Experiments of Chiba University (approval ID: 30-56).

Purification of hematopoietic cells and flow cytometric analysis

Hematopoietic cells harvested from BM were triturated and passed through a 70-µm nylon mesh to obtain a single cell suspension. Cells were incubated with an APC-conjugated anti-c-Kit antibody followed by anti-APC MicroBeads (Miltenyi Biotec). c-Kit$^+$ cells were immunomagnetically enriched by passing through an LS column (Miltenyi Biotec). Purified c-Kit$^+$ cells were then stained with a mixture of biotin-conjugated mAbs against lineage markers, including Gr-1, interleukin (IL)-7Rα, B220, CD4, CD8, and Ter119, and PE-conjugated anti-Sca-1 and APC-conjugated anti-c-Kit antibodies. Biotinylated antibodies were detected with APC-Cy7-conjugated streptavidin. CD45.1

and CD45.2 antibodies were used as additional markers for recipient cells and donor-derived cells, respectively. Flow cytometric analyses were performed using monoclonal antibodies (mAbs) recognizing the following antigens: CD45.2 (104), CD45.1 (A20), Gr-1 (RB6-8C5), CD11b/Mac-1 (M1/70), Ter-119 (TER119), CD71 (RI7217), CD127/IL-7Rα (A7R34), B220 (RA3-6B2), CD4 (RM4-5), CD8α (53-6.7), CD117/c-Kit (2B8), Sca-1 (D7), CD34 (RAM34), CD150 (TC15-12F12 .2), CD41 (MWReg30), and FcγR (93). These mAbs were purchased from BD BioSciences (San Jose, CA), eBioScience (San Diego, CA), and BioLegend (San Diego, CA). Dead cells were eliminated by staining with propidium iodide (1 μg/ml, Sigma). All flow cytometric analyses and cell sorting were performed on FACSAria III and FACSCanto II (BD Biosciences).

Bone marrow (BM) transplantation

BM cells from CD45.2 mutant mice (test cells) were transplanted intravenously into 8- to 12-week-old CD45.1 recipients irradiated at a dose of 9.5 Gy with or without BM cells from 8- to 12-week-old CD45.1 congenic mice (competitor cells). The chimerism of donor-derived hematopoietic cells was monitored by flow cytometry. PB cells were stained with a mixture of mAbs that included Gr-1, Mac-1, B220, CD4, CD8α, CD45.2, and CD45.1. The proportion of donor cells was evaluated by dividing the number of CD45.2-single positive cells by the total number of CD45-positive cells (CD45.1+CD45.2).

Chromatin immunoprecipitation (ChIP) assays and ChIP sequencing

A ChIP analysis was performed as described previously (Mochizuki-Kashio et al., 2015; Tanaka et al., 2017). Cells were cross-linked with 0.5% formaldehyde at 37°C for 2 min,

washed with PBS containing 2% FBS, lysed with ChIP buffer (10 mM Tris-HCl pH 8.0, 200 mM NaCl, 1 mM $CaCl_2$, 0.5% NP40, and protease inhibitor cocktail), and sonicated for 5 sec × 3 times (90 sec on ice) using a Bioruptor (Cosmo Bio). Cells were digested with micrococcal nuclease (MNase) (NEB) at 37°C for 40 min and treated with 10 mM EDTA to stop the reaction. After the addition of an equal volume of RIPA buffer (50 mM Tris-HCl pH 8.0, 150 mM NaCl, 2 mM EDTA, 1% NP40, 0.5% sodium deoxycholate, and 0.1% SDS), cells were resonicated for 5 sec × 10 times (300 sec on ice) using the Bioruptor. After centrifugation, the soluble chromatin fraction was immunoprecipitated at 4°C overnight with Dynabeads M-280 Sheep anti-Rabbit IgG conjugated with an anti-H3K27me3 (07-449, Millipore), anti-H2AK119ub1 (8240, Cell Signaling Technology), or anti-H3K4me3 (07-473, Millipore) antibody. Immunoprecipitates were washed with high salt ChIP buffer (500 mM NaCl) four times and TE buffer (10 mM Tris-HCl pH 8.0 and 1 mM EDTA) twice. Bound chromatin and 25 µl of input DNA were suspended in 47.5 and 22.5 µl of elution buffer (50 mM Tris-HCl pH 8.0, 10 mM EDTA, 1% SDS, and 250 mM NaCl), respectively, and vortexed. After the addition of 5 µl of 5 M NaCl, the solutions were incubated at 65°C for 4 hr and then treated with 25 µg/ml RNase A (Sigma-Aldrich) at 37°C for 30 min and 0.1 mg/ml proteinase K (Roche) at 50°C for 1 hr to reverse formaldehyde crosslinking. Eluted DNA was purified with a MinElutePCR Purification Kit (Qiagen). In ChIP assays, quantitative real-time PCR was performed on input and ChIP DNA samples, as described below. The primer sequences used were as follows. Gene: Forward / Reverse primer (5' to 3').

Cdkn2a: cagggccaaataaagtgctc / tagaaatgagtggccccaac

Pitx1: agtttggaccctctccccta / gcctagagccaacagaaacg

Egr3: cccttccccaaaggaaaata / cccccacacaacttctgtct

Control: caaaaacccctcaaggcata / ggaaaacagcgacttcttgc

In ChIP sequencing, DNA libraries were prepared from input and ChIP DNA samples using a ThruPLEX DNA-seq Kit (Rubicon Genomics) according to the manufacturer's instructions. DNA libraries were quantified using high sensitivity Chip on the Bioanalyzer (Agilent) and sequenced with Hiseq1500 (Illumina) according to the manufacturer's instructions. Sixty-one cycles of sequencing reactions were performed, and sequences were aligned to mouse genome sequences (mm10) using the Eland program. Sequences allowing no more than two mismatches per sequence were used for the analysis. The reads per million mapped read (RPM) values of the sequenced reads were calculated every 2,000-base pair bin with a shifting size of 200 base pairs using bed tools and normalized with the amount of ChIP DNA in the H3K27me3 analysis. In order to evaluate the histone modification mark of each gene, the RPM values of the region from 2 kb upstream to 2 kb downstream of the TSS of the immunoprecipitated samples were divided by the RPM of the corresponding input. In order to visualize with the Integrative Genomics Viewer (IGV) (http://www.broadinstitute.org/igv), the RPM values of the immunoprecipitated samples were normalized by subtracting the RPM values of the input samples in each bin and then converted to a bigwig file using the wigToBigWig tool. The super-computing resource was provided by the Human Genome Center, the Institute of Medical Science, the University of Tokyo (http://sc.hgc.jp/shirokane.html).

RNA sequencing (RNA-seq)

An RNA-seq analysis was performed as described previously (Mochizuki-Kashio et al., 2015; Tanaka et al., 2017). Total RNA was subjected to reverse transcription and amplification with the SMARTer Ultra Low Input RNA Kit for Sequencing (Clontech).

After sonication with an ultrasonicator (Covaris), the libraries for RNA-seq were generated from fragmented DNA with 8 cycles of amplification using a NEB Next Ultra DNA Library Prep Kit (New England BioLabs). After the libraries had been quantified using the Bioanalyzer (Agilent), samples were subjected to sequencing with Hiseq1500 (Illumina) and 61 cycles of the sequencing reactions were performed. TopHat2 (version 2.0.13; with default parameters) and Bowtie2 (version 2.1.0) were used for alignment to the reference mouse genome (mm9 from the University of California, Santa Cruz Genome Browser; http://genome.ucsc.edu/). Gene expression values were then calculated as reads per kilobase of exon units per million mapped reads (RPKM) using cufflinks (version 2.2.1).

Western blotting

Cells were lysed in 2×SDS sample buffer, sonicated with the Bioruptor (Cosmo Bio), and boiled at 95°C for 10 min. Proteins in lysates were separated by SDS-PAGE, transferred to a PVDF membrane, and detected by Western blotting using the following antibodies: anti-histone H3 (ab1791, Abcam), anti-H3K27me3 (07–449, Millipore), anti-H3K27me2 (9755S, Cell Signaling Technology), anti-H3K27me1 (07–448, Millipore), anti-H3K27ac (ab4729, Abcam), anti-histone H2A (ab18255, Abcam), and anti-H2AK119ub (8240S, Cell Signaling Technology). Protein bands were detected with enhanced chemiluminescence reagent (Immobilon Western, Millipore). The sequential reprobing of membranes with antibodies was performed after the removal of primary and secondary antibodies from membranes in 0.2 M glycine-HCl buffer (pH 2.5) and/or the inactivation of HRP by 0.1% NaN_3.

Quantitative RT-PCR for the gene expression analysis

Total RNA was isolated using TRIZOL LS solution (Invitrogen, Carlsbad, CA) or the SMARTer Ultra Low Input RNA Kit for Sequencing (Clontech) and reverse-transcribed using the ThermoScript RT-PCR system (Invitrogen) or ReverTra Ace (Toyobo). Quantitative real-time PCR was performed with a StepOnePlus Real-Time PCR System (Life Technologies) using TB Green™ Premix Ex Taq™ II (Takara Bio). The primer sequences used were as follows. Gene: Forward / Reverse primer (5' to 3').

Cdkn2a (*p19*): gggttttcttggtgaagttcg / ttgcccatcatcatcacct

Pitx1: atcgtccgacgctgatct / ttcttagctgggtcctctgc

Egr2: ctacccggtggaagacctc / aatgttgatcatgccatctcc

Egr3: caatctgtaccccgaggaga / ccgatgtccatcacattctct

Tbx15: cactcggagacacagacgac / gagtccgacccagtgctc

Htra1: cattgaagtcattcctgacacc / tgtccgttgatgctgatga

Hprt: tcctcctcagaccgctttt / cctggttcatcatcgctaatc

Lentiviral vectors and virus production

Full-length mouse *Pitx1*, *Egr2*, *Egr3*, *Tbx15*, and *Grb10* cDNA obtained from DKO LSK cells and tagged with 3×FLAG at the N terminus were subcloned into the CSII lentiviral expression vector, which contained an internal ribosomal entry site (IRES) upstream of the Venus as a marker gene. A recombinant lentivirus was generated in 293T cells. The virus in 293T cell supernatants was concentrated by centrifugation at 6,000 *g* for 16 hours.

Statistical analysis

144 The significance of differences was measured by an unpaired two-tailed Student's *t*-test
145 or Welch's *t*-test when variance was judged to be significantly different by the F-test.
146 These tests were performed using Excel (Microsoft). **p*<0.05, ***p*<0.01, ****p*<0.001,
147 NS, not significant.
148

149 **Deposition of data**

150 RNA sequence and ChIP sequence data were deposited in the DNA Data Bank of Japan
151 (DDBJ**:** DRA007027).
152

153 **References**

154 Bae W.K., Kang K., Yu J.H., Yoo K.H., Factor V.M., Kaji K., Matter M., Thorgeirsson
155 S. and Hennighausen L., The methyltransferases enhancer of zeste homolog (EZH) 1 and
156 EZH2 control hepatocyte homeostasis and regeneration, FASEB J. 29, 2015, 1653–1662
157 Hirabayashi Y., Suzki N., Tsuboi M., Endo T.A., Toyoda T., Shinga J., Koseki H., Vidal
158 M. and Gotoh Y., Polycomb limits the neurogenic competence of neural precursor cells
159 to promote astrogenic fate transition, Neuron 63, 2009, 600–613.
160 Tanaka T., Nakajima-Takagi Y., Aoyama K., Tara S., Oshima M., Saraya A., Koide S.,
161 Si S., Manabe I., Sanada M., et al., Internal deletion of BCOR reveals a tumor

162 suppressor function for BCOR in T lymphocyte malignancies, J. Exp. Med. 214, 2017,
163 2901–2913.